Constitutive model for small rock joint samples in the lab and large rock joint surfaces in the field

R. E. Barbosa
EngSolutions, Inc., Ft. Lauderdale, Florida, USA

ABSTRACT: A new constitutive model for rock joints is proposed for predicting the mechanical behavior of both small joint samples in the lab and large joint surfaces in the field. The normal and shear behavior of joints samples is predicted based on the strength and geometry of small-scale joint asperities. The behavior in the field is predicted based on the strength of small-scale asperities, determined from lab data, and the geometry of field-scale waviness determined from geologic observations. The concept of available shear strength is introduced to describe the degradation of asperities and the shape of the mobilized shear stress-displacement curve. Dilation and roughness degradation during shear is correlated to a dimensionless product of shear stress, incremental displacement, rock strength, and wavelength of irregularities. Instead of using any scaling procedures, the behavior of joints in the field is predicted by applying the model for lab samples to the actual contact areas developed in large-scale joint surfaces.

1 INTRODUCTION

Numerous models have been proposed to describe the mechanical behavior of rough joints. One of the earliest models for peak shear strength is Patton's (1966), which is based on the basic mechanics of either sliding up the asperity or shearing through the asperity, depending on the normal stress level. Similar models were proposed later providing a curved transition from dilation to shearing, including Ladanyi's (1970) and Jaeger's empirical model (1971). More complicated models appeared later, which relate the roughness angle with the normal stress, including Schneider's (1976), Barton's empirical model (1977), and Plesha's theoretical model (1987). Other models relating roughness to different parameters have been proposed; including models based on statistical parameters, such as Reeves (1985), models based on fractal analysis such as Lee's (1990) and Kulatilake's (1995), and models based on three-dimensional surface parameters, including Grasselli's (2003) and Belem's models (2007). Among all models proposed, Barton's criterion is the one most widely used in practice. Such model and most of the above joint models are focused on the peak shear strength.

Extrapolation of the mechanical behavior of lab-scale joint samples to large-scale surfaces in the field has also been the subject of numerous investigations. Various authors have reported scale effects on the shear strength of joints. Pratt (1974), Bandis (1980) and Hencher (1993) observed a reduction in peak shear strength with increasing joint size. However, other authors, including Leal-Gomez (2003) and Fardin (2003) have presented cases showing the opposite behavior.

In practice, the mechanical behavior of rock joints in the field is often estimated on the basis of parameters determined on small joint samples, which are either scaled or assumed to be retained through scale magnifications. Such approaches are based on the assumption that the geometry of large-scale irregularities, not present in the lab sample, is in some way related to the geometry of small-scale irregularities present in the lab sample. However, these geometries

are not necessarily related as they are often determined by completely different factors. The roughness profile of a natural joint in granite for instance is determined by the size and distribution of the rock-forming grain minerals, while the large-scale waviness profile is determined by the geologic or tectonic process that created the joint.

In the proposed model, the behavior of rock joints in the field is determined based on the strength and geometry of small-scale joint roughness determined from lab data, and the geometry of field-scale waviness determined from geologic observations. The proposed model is not a new shear strength criterion suitable for hand calculations such as limit equilibrium analysis. It is a complete fully incremental model that allows predicting the normal and shear behavior of unfilled joints subjected to general non-monotonic unidirectional loading, suitable for numerical analysis, including finite element analyses and discrete element analyses.

2 ASPERITY DEGRADATION

Asperities are damaged during shearing, which results in a progressive reduction of the effective asperity angle. Damage to asperities involves various mechanisms including wearing, grinding, breaking and crushing. Observations on sheared samples reveal that the extent of the degradation depends on various factors. Greater degradation occurs for larger shear displacements, higher normal stresses, lower strength of asperities, and for joints with sharper and smaller asperities.

Various models have been proposed to describe roughness degradation. Barton (1982) developed the concept of mobilized roughness so that shear stress-displacement curves could be modeled, normalizing the degradation of roughness. Based on his shear strength criterion, a mobilized joint roughness coefficient (JRC) is computed along all points of the shear displacement plot and both the JRC_{mob} and displacement are normalized to peak values. The model is used as a table of normalized JRC versus normalized displacement values.

Plesha (1987) proposed an exponential degradation of the asperity angle α, as follows:

$$\alpha = \alpha_0 e^{-cW_p} \tag{1}$$

where α_0 = initial asperity angle, c = degradation constant, W_p = plastic work done in shear = $\Sigma\, \tau.d\delta_s^p$, τ = shear stress, δ_s^p = plastic displacement.

Various authors have investigated experimentally Plesha's model, which is theoretically complete and highly adaptable to numerical implementation. Hutson and Dowing (1990) proposed an equation for the degradation constant. Huang et al (1993) validated the model for saw-tooth joints. Lee et al (2001) proposed extended versions of the model for cyclic loading. Oh (2005) evaluated existing equations for the degradation constant, and proposed an equation that accounts for the size and strength of the asperity and fits well experimental data on replicas of natural joints.

3 PARAMETERS OF THE PROPOSED MODEL

The main parameters of the proposed model are as follows. The basic friction is characterized by the residual friction angle ϕ_r. Lab-scale asperities are characterized by the initial average asperity angle α_0, asperity wavelength λ, and the asperity compressive strength σ_c. Field-scale waviness is characterized by the initial average waviness angle i_0 and the waviness wavelength λ_w.

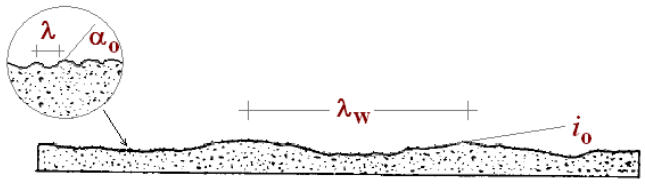

Figure 1. Parameters of proposed model.

4 SHEAR BEHAVIOR

The shear stress-displacement curve generated by the proposed model includes 3 stages, illustrated in Fig. 2: (1) mobilization of basic shear, (2) mobilization of peak strength, and (3) mobilization of residual strength.

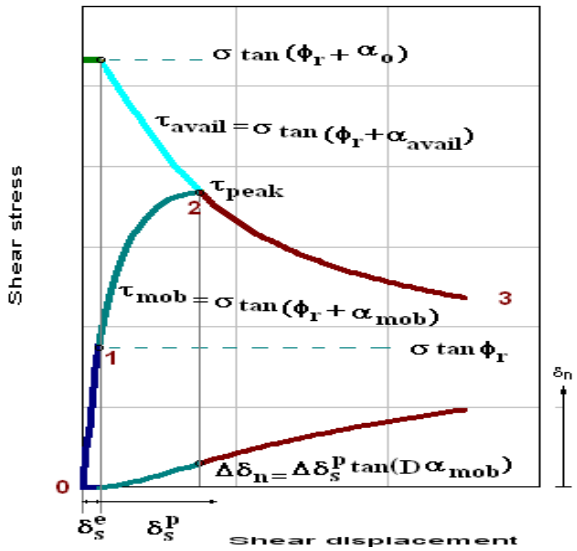

Fig. 2. Available shear strength-displacement, mobilized shear stress-displacement and dilation curves of proposed model

In order to describe the shape of the shear stress-displacement curve, the concept of available shear strength is introduced. Available shear strength is the strength the joint would have at any stage if there were no additional degradation (i.e. shear strength for current joint geometry).

In a deformation controlled direct shear test on a joint sample the basic friction is mobilized first. This initial stage is assumed to be elastic. The shear stress is mobilized as a function of the joint shear stiffness (K_{si}). The displacement required to mobilize the full basic friction ($\sigma \tan \phi_r$) is the elastic displacement δ_s^e. In this stage, there is no degradation. Hence the available shear strength is equal to $\sigma \tan (\phi_r+\alpha_0)$.

After the elastic region, the joint starts to slide over the asperities, initiating degradation and dilation. The shear displacements at this stage are plastic displacements. As the mobilized shear increases, asperities get damaged, the average asperity angle decreases, and hence, the available shear strength decreases. The peak strength is reached when the mobilized shear becomes equal to the available shear strength.

After the peak, the mobilized shear stress continues being equal to the available strength, which continues to degrade.

In both the pre-peak and the post-peak plastic zones the vertical displacement can be computed incrementally based on the plastic shear-displacement and the dilation angle. The dilation angle is computed as fraction D of the mobilized asperity angle. The factor D is around 0.5 as observed by Barton (1982) and Oh (2005).

4.1 *Proposed degradation model*

In the proposed incremental degradation model, the decrement in asperity angle $d\alpha$, produced when a joint with a current asperity angle α, under a shear stress τ, undergoes an incremental sliding displacement $d\delta_s^p$, is

$$d\alpha = -\frac{\kappa}{\lambda.\sigma_c}\alpha.\tau.d\delta_s^p \qquad (2)$$

where, κ is a fitting constant. For higher normal stresses a larger shear stress is required to produce sliding. Thus, according to Eq. (2) rough joints with small and weak asperities subject to

high normal stresses degrade faster. For replicas of various naturals joints used to validate the proposed model, κ was found to be in the range 10 to 15.

For monotonic loading, integration of Eq (2) yields equation Eq (1) with $c = \kappa/\lambda.\sigma_c$. Hence, Plesha's model is included in the proposed incremental degradation model.

4.2 *Elastic region*

The increment of mobilized shear is computed based on the shear stiffness as $\Delta\tau = K_{s_i}.\Delta\delta_s^e$. In this stage there is neither degradation nor dilation, thus, the decrement in the asperity angle is nil. The elastic joint shear stiffness is estimated as

$$K_{s_i} = \sigma_c \tan\phi_r / C \tag{3}$$

where C is a fitting constant that varies between 0.7 mm (replicas on hard material σ_c > 80 MPa) and 4 mm (joint models on soft material σ_c = 2 MPa)

4.2 Pre-peak plastic region

The increment of mobilized shear is computed using a tangent shear stiffness as $\Delta\tau = K_t.\Delta\delta_s^p$. The decrement in the asperity angle is computed using the proposed degradation law as $\Delta\alpha = -\kappa/\lambda\sigma_c.\alpha_{avail}.\tau_{mob}.\Delta\delta_s^p$. The increment of normal displacement is computed based on the dilation angle, which is taken as a fraction of the mobilized asperity angle, i.e. $\Delta\delta_n = \Delta\delta_s^p.\tan(D\alpha_{mob})$.

Updated mobilized shear stress and available shear strength are computed as follows:

$$\begin{aligned} \tau_{mob} &= \tau_{mob}^{old} + \Delta\tau & \alpha_{avail} &= \alpha_{avail}^{old} + \Delta\alpha \\ \alpha_{mob} &= \tan^{-1}(\tau_{mob}/\sigma) - \phi_r & \tau_{avail} &= \sigma\tan(\phi_r + \alpha_{avail}) \end{aligned} \tag{4}$$

The tangent joint shear stiffness is determined assuming a hyperbolic shear stress-relation in the pre-peak plastic region, thus:

$$K_t = K_{s_i}(1 - R_f\,\tau_{mob}/\tau_{avail})^2 \tag{5}$$

where R_f, the ratio between the actual available strength and the asymptotic (hyperbolic) strength, varies between 0.7 and 0.9.

4.3 Post-peak softening region

In this region the available shear strength is fully mobilized. The decrement in the asperity angle and incremental normal displacements are computed as above, the updated available shear strength is $\tau_{avail} = \sigma\tan(\phi_r + \alpha_{avail})$ and updated mobilized shear $\tau_{mob} = \tau_{avail}$.

5 NORMAL LOADING BEHAVIOR

Various authors have investigated the deformation of joints under normal loading. A notable work is the extensive experimental program conducted by Bandis et al (1983), which included numerous loading/unloading and repeated load cycling tests on a wide variety of fresh and weathered joints in different rock types. Based on their test data, they proposed a hyperbolic equation to describe the normal stress-closure curves of rock joints, which in incremental form is written as follows:

$$d\sigma_n = K_{n_i}\left(1 - \frac{\sigma_n}{K_{n_i}\delta_{mc} + \sigma_n}\right)^{-2} d\delta_n \tag{6}$$

where, K_{ni} = initial normal stiffness and δ_{mc} = maximum joint closure. The above hyperbolic normal stress-join closure relation is used in the present model and procedures are proposed to determine the equation parameters.

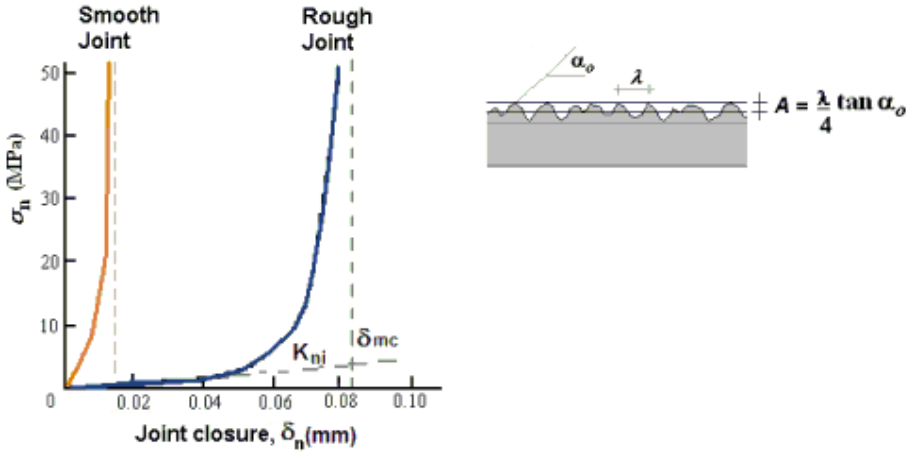

Fig. 3. Normal- stress-closure curves for rock joints

5.1 *Maximum joint closure*

Comparing the stress-deformation relation of rough joints and smooth joints with similar joint compressive strength, as illustrated in Fig. 3, it is observed that the maximum closure of rough joints is greater than that of smooth joints. If compression tests are not available, it seems reasonable to assume that the maximum closure could be estimated as a fraction of the amplitude of asperities, A. Therefore, it is proposed to estimate the maximum closure as follows:

$$\delta_{mc} = f.\lambda.\tan\alpha_0 \tag{6}$$

For the first loading cycle (virgin compression) of interlocked joints, the factor f is about 0.1 for fresh joints and about 0.2 for weathered joints. In general, f depends on σ_c and the loading history.

Using Bandis et al (1983) data, the variation of f with σ_c was obtained for virgin loading (f_l), reloading (f_r) and unloading (f_u), as shown in Fig. 4. The points for high values of σ_c correspond to fresh joints while the points for low σ_c values are for weathered joints. For the same joint geometry, during virgin loading, a smaller δ_{mc} is reached for stronger asperities. For unloading and reloading, the factor f is practically independent of the strength of asperities. Thus, the factor f can be estimated as shown in Fig. 4.

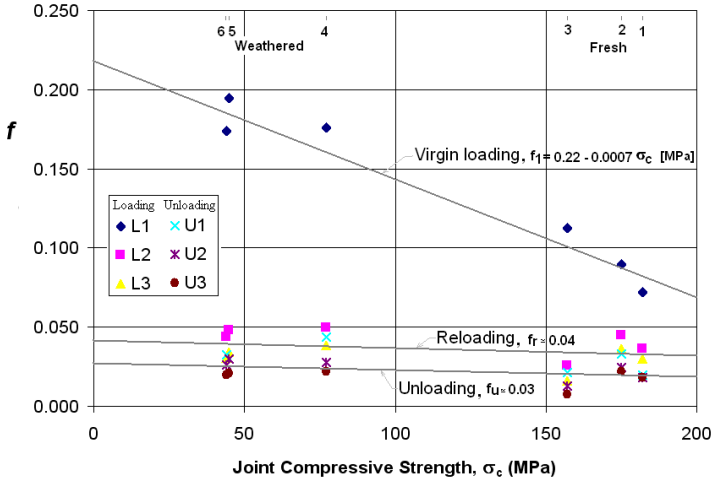

Fig. 4. Fitting parameter f. (1:Fresh dolerite, 2:fresh slate, 3: fresh limestone, 4: weathered slate, 5:weathered siltstone, 6: weathered limestone)

5.2 *Initial normal stiffness*

When a normal stress σ_n is applied to a rock joint, the tips of the asperities crush and deform plastically until a contact area a_c is developed such that the contact stress becomes equal to the compressive strength of the asperity σ_c.

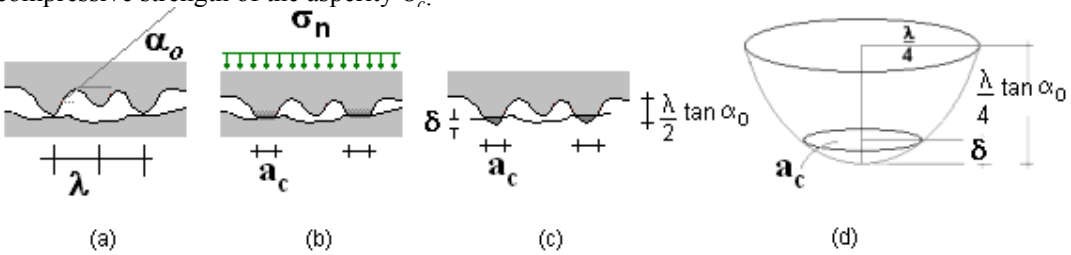

Fig. 5.Development of contact area during normal loading and contact area for a paraboloidal asperity

The contact area at the tip of the asperity is $a_c = \sigma_n \lambda^2 / \eta \sigma_c$, where, η is the ratio between the number of asperities in contact and the total number of asperities. A relation between the deformation and the contact area can be obtained based on the shape of the asperity. For instance, for a paraboloidal asperity the area of contact after a penetration δ is $a_c = \pi \lambda \delta / 4 \tan \alpha$. Combining these two equations yields the following normal stress-closure relation:

$$\sigma_n = \frac{\pi \sigma_c \eta}{4 \lambda \tan \alpha} \delta_n \tag{7}$$

During normal compression of rock joints, as the normal displacement δ_n is increased, the ratio η increases as new asperities get into contact, and the average angle α decreases as asperities get crushed, which produce the nonlinear stress-closure relation. Differentiating Eq. (7) yields the following equation for the initial normal stiffness K_{ni}:

$$K_{ni} = \tfrac{\pi}{4} \eta_o f \frac{\sigma_c}{\delta_{mc}} \tag{8}$$

If 2D triangular asperities are considered instead of 3D paraboloidal asperities, an equation similar to Eq. (8) but with a coefficient equal to 2 is obtained. Thus, for ideal paraboiloidal and triangular asperities the normal stiffness is directly proportional to the compressive strength of the asperity and inversely proportional to the maximum closure. Therefore, it is proposed to estimate the initial normal stiffness for real joints as follows:

$$K_{ni} = \frac{\sigma_c}{\Omega \delta_{mc}} \tag{9}$$

where, Ω is a fitting parameter.

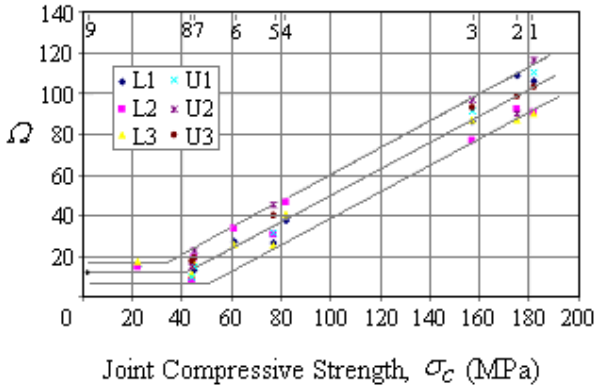

Fig. 6. Fitting parameter Ω (1:Fresh dolerite, 2:fresh slate, 3: fresh limestone, 4: fresh sandstone, 5: weathered slate, 6: moderately weathered sandstone, 7:weathered siltstone, 8: weathered limestone, 9: model joint)

Using Bandis et al (1983) data, the fitting parameter Ω was computed for various joint types and degrees of weathering. As shown in Fig. 6 the parameter Ω, which allows computation of the initial normal stiffness, is a function of the strength of the joint material. The points included in Fig. 6 include those computed from normal stiffness and maximum closure for: first loading (L1: virgin loading), first unloading (U1), second loading (L2: reloading), second unloading (U2), 3rd loading (L3) and 3rd unloading (U3). They all follow the same pattern, which means that the product ($K_{ni}.\delta_{mc}$) is essentially the same for virgin loading, unloading and reloading. The Ω factor can be estimated as follows:

$$\Omega = -13.6 + 0.64\sigma_c[MPa] \geq 12 \tag{10}$$

5.3 *Asperity degradation during normal loading*

While many authors have studied degradation during shear loading, degradation during normal loading is rarely discussed. An equation for the decrement of asperity angle can be obtained by differentiating the equation for the amplitude of asperities $A = ¼\ \lambda\ tan\ \alpha$. The decrement of the amplitude of asperities is equal to the plastic joint closure, thus:

$$d\alpha = -\frac{4\cos^2\alpha}{\lambda} d\delta_n^p \tag{11}$$

The plastic closure during virgin loading is the difference between the total closure and the elastic rebound, and it is computed as follows:

$$d\delta_n^p = d\delta_n - d\delta_n^e = (1 - f_u / f_1) d\delta_n \tag{12}$$

6 FIELD BEHAVIOR

While available shear strength resistance of lab-scale joint samples include two components, basic friction and roughness, in the field there is an additional component, the large-scale waviness. Still, the shear strength in the field is smaller than in the lab. In previous works this behavior has been explained by arguing that in the field the effective asperity angle is smaller than in the lab due to 'scale effects'. However, since the surface texture of the joint is the same in the field and in the lab, it is not clear why the roughness is smaller in the lab.

In the proposed model, the above behavior is explained differently. There are no scale effects and the size of the sample is not a significant parameter in the proposed model. It is postulated that the initial asperity angle is the same in the lab and in the field. However, due to the presence of waviness in the field, the asperity angle is degraded much faster, as damage to asperities is concentrated in small contact areas, subjected to magnified contact stresses.

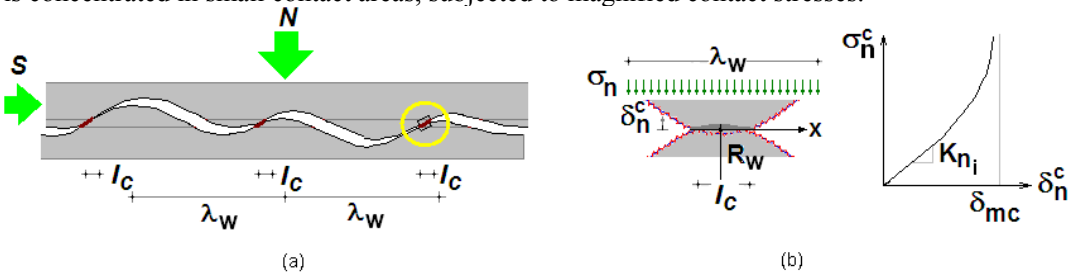

Fig. 7. (a) Reduced contact area due to waviness (b) contact area and contact stress-closure relation

6.1 *Contact area ratio*

As illustrated in Fig. 7(a), when shearing is initiated, the joint surface gets mismatched and the contact area is reduced significantly. Let a =ratio of contact area to total area, i.e. $a = A_c/A_t = \eta l_c/\lambda_w$, where η = ratio of number of 'waves' in contact to total number of 'waves'. The con-

tact stresses can be written in terms of the applied overall stresses and the contact area ratio as follows:

$$\sigma^c = \sigma_n / a$$
$$\tau^c = \tau_s / a \tag{13}$$

And, the rate of degradation of asperities becomes

$$\Delta\alpha = -\frac{\kappa}{\lambda\sigma_c}\alpha.\tau_s.\Delta\delta_s^p / a \tag{14}$$

Therefore, for a contact area ratio of about 10%, as observed by Pratt et al (1974), the contact stresses are magnified by a factor of 10 and the degradation rate becomes 10 times faster.

In the proposed model, the behavior in the field is determined by applying to the contact area, the behavior observed in the lab. Based on the contact area ratio, a, the applied overall normal stresses are transformed into contact stresses, and mobilized shear stresses occurring at the contacts are translated into overall stresses using Eq. (13).

An equation for the contact area ratio, for a contact point on the waviness profile with radius of curvature R_w, illustrated in Fig. 7(b), can be obtained based on the normal stress-closure relation at the contact, by assuming a parabolic distribution of the normal deformation δ_n^c.

If a linear normal stress-closure defined by a normal stiffness K_{ni} is assumed, equilibrium yields:

$$\sigma_n \frac{\lambda_w}{\eta} = 2\int_{-l_c/2}^{l_c/2} K_{ni}.\delta_n^c(x).dx = \frac{K_{ni} l_c}{6R_w} \tag{15}$$

Thus, the contact area ratio $a = A_c/A_t$, is given by

$$a = \left(\frac{6\sigma_n R_w \eta^2}{K_{ni}\lambda^2}\right)^{1/3} \tag{16}$$

If a more realistic hyperbolic normal stress-closure relation at the contact is assumed, the following cubic equation for the contact area ratio is obtained:

$$a^3 + a^2 \frac{\sigma_n}{2K_{ni}\delta_{mc}} = \frac{6\sigma_n R_w \eta^2}{K_{ni}\lambda^2} \tag{17}$$

The waviness angle i, and the radius of curvature R_w, vary along the waviness profile. For a perfect sinusoidal profile, the initial point of contact would be the point at which the waviness angle is maximum. However, for a more realistic profile as that illustrated in Fig. 7, the initial point of contact at some 'waves' would be near the point where the waviness angle is equal to the average value (i_o) while for other 'waves' the point may be below this point and for other 'waves' the initial contact may be above it. In this study, for computing the initial contact area ratio, it is assumed that on the average, the initial point of contact occurs at the point in the profile where the waviness angle is equal to the average waviness angle. The radius of curvature at such location is $R_w = 0.13\ \lambda_w/\tan i_o$.

6.2 *Contact parameter* η

The parameter η in Eq. (15) is not important in the field where there are numerous 'waves' thus it can be assumed to be equal to 1.0. However, in most experimental programs conducted to study scale effects, where the number of 'waves' varies between 1 and 3, the η parameter becomes important. This parameter reflects the relative concentration of stresses at contacts, and it explains inverse scale effects that have been observed (e.g. Leal Gomez 2003, Fardin 2003). Consider a 90 cm rock joint with waviness wavelength λ_w = 30 cm, from which replicas of different lengths are prepared and sheared as shown in Fig. 8. For a 36 cm sample there are two contact points and η=2/(36/30) = 1.66. For a 45 cm sample, there are also two contact points

and η=2/(45/30) = 1.33. For the same overall normal stress, contact stresses in the 45-cm long sample are larger, thus degradation is faster and the resulting shear strength is smaller. For a 70 cm-long there are still only 2 contacts, thus for the same overall normal stress even larger contact stresses would develop and lower shear strength would be obtained (η=0.85). Next, if the length of the sample were increased to 75 cm, there would be 3 contacts. For the same overall normal stress the contact stresses would be smaller than those for the 70-cm long sample, resulting in slower degradation and larger shear strength (η=1.20). Thus it is not the length of the sample *per se* what produces the 'scale effects' but the relative concentration of stresses, which is measured by the parameter η.

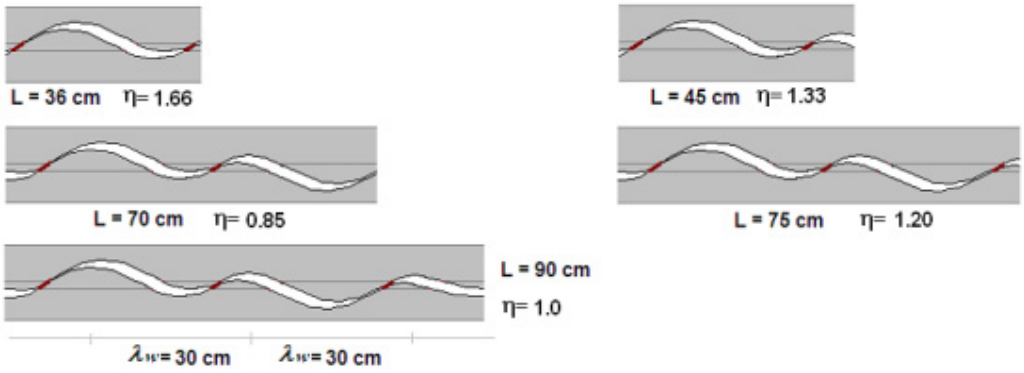

Fig. 8. Contact parameter η

6.3 *Open joints*

Rock mass failures often occur along joints that are under low normal stresses and have opened and mismatched. The strength of those open joints is between that of a tightly closed joint and that of a completely dislocated joint. Interlocking and thus strength is larger for the locked joint because the initial effective waviness angle is larger, the contact parameter η is larger, the effective radius of curvature at the contact point is larger, and thus the contact area ratio is larger.

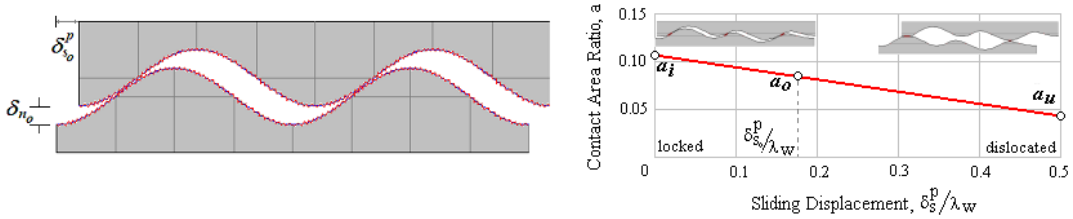

Fig. 9. Contact ratio for open joints

An equivalent initial shear displacement value can be computed based on the joint aperture, in order to interpolate for initial values of contact area ratio and waviness angle, as illustrated in Fig. 9, by assuming a sinusoidal waviness profile. The equivalent initial shearing displacement is computed as follows:

$$\frac{\delta_{s_0}^{p}}{\lambda_w} = \frac{1}{\pi} Sin^{-1}\left(\frac{2\delta_{n_0}}{\lambda_w \tan i_0}\right) \tag{18}$$

6.4 *Shear stress displacement curve*

The shear stress-displacement curve for a large joint surface in the field includes the same three regions defined for a small sample in the lab: elastic region, pre-peak region and post-peak plastic region. The proposed lab-scale model is applied to the contact area and contact stresses are converted to overall values, using Eq. (13), to determine the field stress-displacement curve in these regions. Thus, for the elastic region, as basic friction is mobilized, if the applied overall

normal stress is σ_n, the normal stress at the contact would be $\sigma_n^c = \sigma_n / a_o$. The increment of mobilized shear stress at the contact is $\Delta\tau^c = K_s.\Delta\delta_s$, hence the overall increment of mobilized shear stress would be $\Delta\tau = a_o.K_s.\Delta\delta$. Therefore, the equivalent shear stiffness in the field is equal to

$$K_{field} = a_o.K_s \tag{19}$$

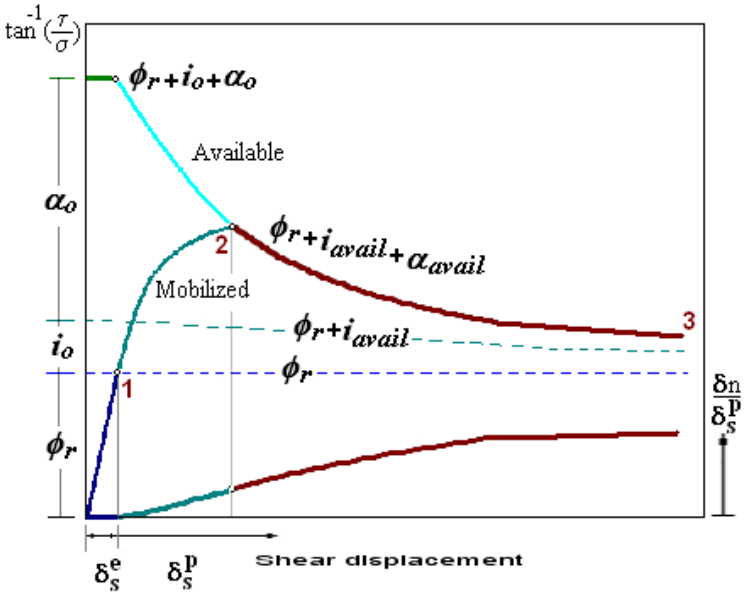

Fig. 10. Available and mobilized friction angle Vs. shear displacement for large joint surfaces in the field

In the pre-peak and post-peak plastic regions, the joint slides over the asperities at small contact areas, degrading them and dilating as the contact point climbs up the waviness, producing some degradation to the waviness, and reaching points on the profile with lower effective waviness angle, which reduces de contact area ratio. Degradation of asperities is computed as follows:

$$\Delta\alpha = -\frac{\kappa}{\lambda\sigma_c}.\alpha_{avail}.\tau / a.\Delta\delta_s^p \tag{20}$$

Thus degradation of asperities in the field goes much faster than in the lab due to the factor *1/a*. A similar degradation law is assumed for waviness and a geometric term is added to reduce the effective waviness angle, from the initial average value to *0* after a shear displacement of $0.5\lambda_w$. Thus,

$$\Delta i = -\frac{\kappa}{\lambda_w\sigma_c}.i_{avail}.\tau.\Delta\delta_s^p - \frac{2i_0}{\lambda_w}\Delta\delta_s^p \tag{21}$$

Since the wavelength of waviness is considerable larger than that of asperities and overall stresses are significantly smaller than contact stresses, degradation of waviness is minimal as compared to degradation of asperities, even after adding the geometrical term.

Under constant normal stress, the contact area ratio changes during shear displacement as illustrated in Fig. 9, from an initial value a_i to an ultimate value a_u for the fully dislocated configuration. The change of contact area ratio due to changes in normal stress is determined from the partial derivative of Eq. (17). Thus Δa is computed as follows:

$$\Delta a = -\frac{2(a_i - a_u)}{\lambda_w}\Delta\delta_s^p - \frac{a}{3+\frac{\Omega}{a}\frac{\sigma_n}{\sigma_c}}\frac{\Delta\sigma_n}{\sigma_n} \tag{22}$$

7 APPLICATION EXAMPLES

The proposed model was verified using experimental data from the literature that provides detailed stress-displacement curves, material parameters and joint profiles.

7.1 *Simulation of Flaman* et al*'s test*

Flamand *et al* (1994) conducted direct shear tests on identical replicas of a natural fracture in granite under three normal stresses. The characteristics of the mortar used are $\phi_r = 37°$ and $\sigma_c = 82$ MPa. The samples are circular 90 mm in diameter. Joint profiles recorded parallel to the shear direction are presented in Fig. 11. Based on these profiles the average wavelength of asperities was determined to be $\lambda = 3$ mm.

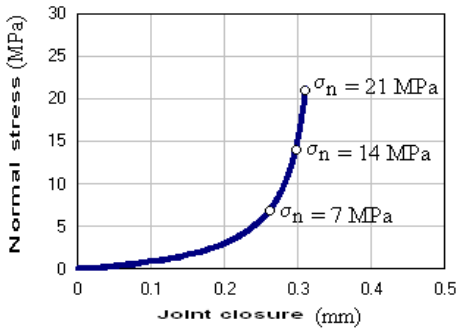

(a) Application of normal stress

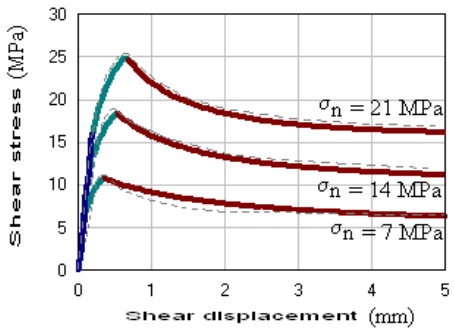

(b) Shear displacement curves

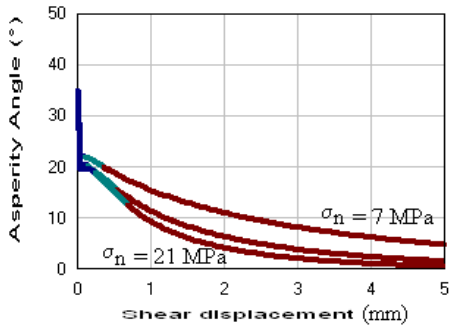

(c) Asperity degradation

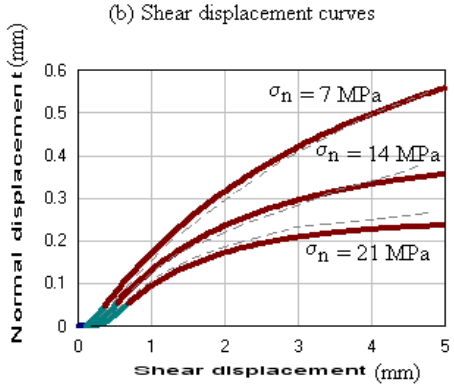

(d) Normal-shear displacement curves

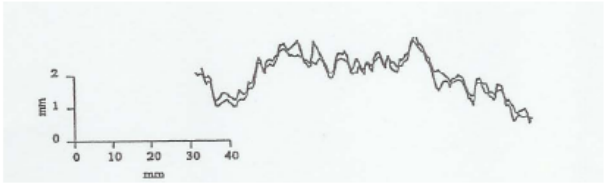

(e) Joint wall profile

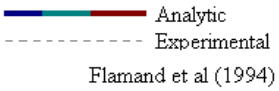

(f) Input parameters used in simulation

ϕ_r (o)	α_o (o)	λ mm	σ_c MPa
37	35	3	82

(g) Fitting constants

C mm	f_1 –	Ω –	R_f –	D –	κ –
0.7	0.163	38	0.7	0.6	10

Fig. 11. Comparison between proposed model and test results (experimental data from Flamand, 1994)

Figure 11 shows a comparison between simulation results and experimental results. The initial asperity angle $\alpha_0 = 35°$ was back calculated from the peak-strength for the test with lowest normal stress (7 MPa), adding the degradation under shear and that under normal loading. The tests

for intermediate and high normal stresses were entirely predicted based on the above four parameters. The proposed model provides a very good correlation with the experimental data.

7.2 *Simulation of Bandis' tests*

Bandis (1980) conducted systematic studies of the scale effects on the shear strength of joints by performing direct shear tests on different sized replicas cast from various natural surfaces, including full size joints (36 or 40 cm) and joints cut into smaller segments. The model joint compressive strength was σ_c = 2 MPa, the basic friction angle was ϕ_b = 32° and the normal stress for all tests was σ_n = 24.5 Kpa.

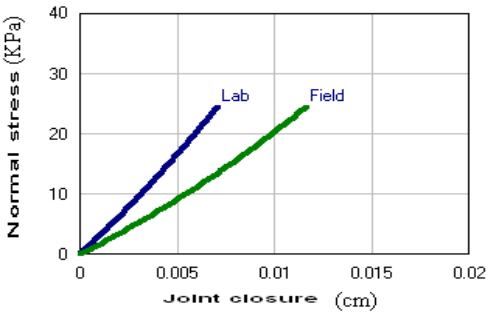

(a) Application of normal stress

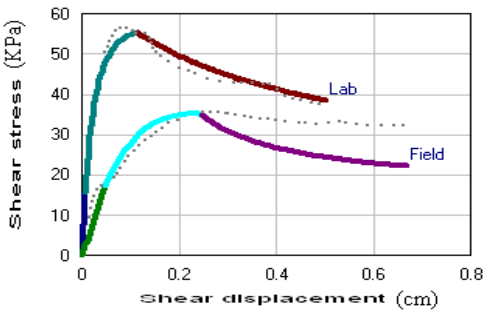

(b) Shear displacement curves

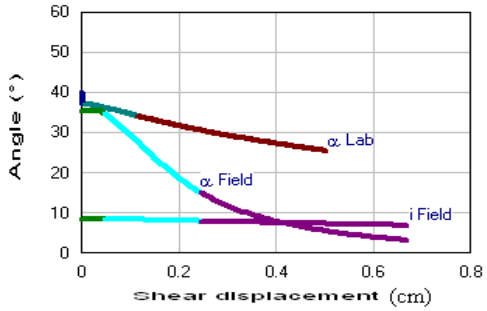

(c) Asperity degradation

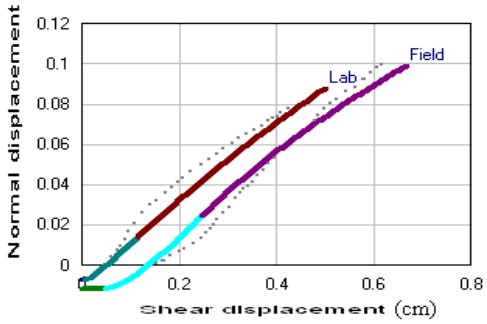

(d) Normal-shear displacement curves

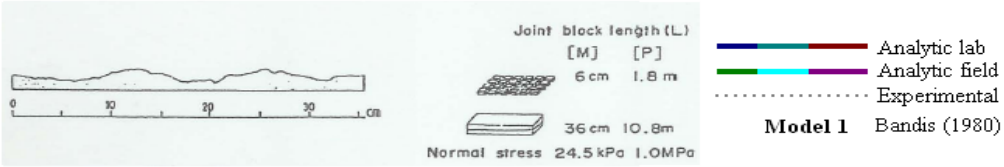

(e) Joint wall profile

(f) Input parameters used in simulation

Sample size cm	ϕ_r (o)	α_o (o)	λ cm	σ_c KPa	i_o —	λ_w —	η_1 —
6	32	40	0.3	2000	—	—	—
36	32	40	0.3	2000	8.5	10	0.83*

(g) Fitting constants

C cm	f_1 —	Ω —	R_f —	D —	κ —
0.4	0.219	12	0.9	0.37	10
0.4	0.219	12	0.9	0.37	10

* 3 contacts / (36/10) waves = 0.83

Fig. 12 Comparison between proposed model and test results (experimental data from Bandis, 1980)

Most of Bandis's tests were simulated in this study and the agreement between the model predictions and experimental results was always good. Fig. 12 shows simulation for one of the

model joints (Model No 1). Results are presented for joint size 6 cm (Lab) and for joint size 36 cm ("Field"). Wavelength for both small scale and large-scale irregularities along with waviness angle (i_o) were determined from a set of three surface profiles for each model. Initial asperity angle (α_o) was back- calculated from the tests results. Figure 13 shows simulation for a second model joint (Model No. 2).

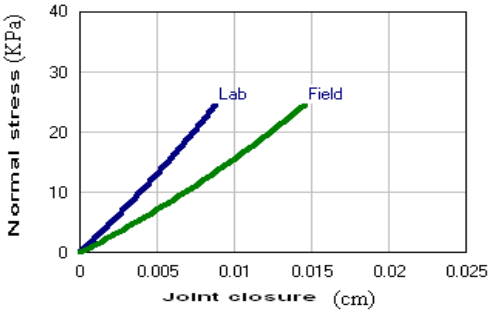

(a) Application of normal stress

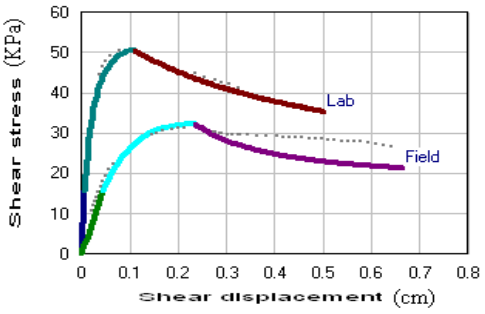

(b) Shear displacement curves

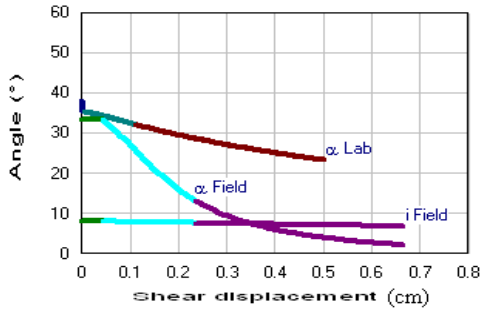

(c) Asperity degradation

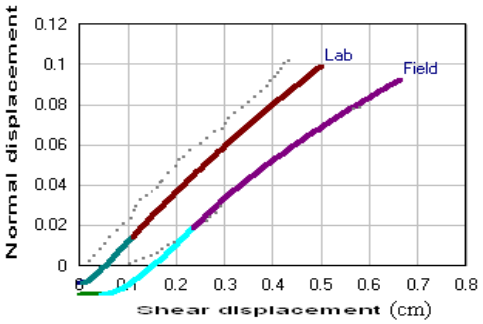

(d) Normal-shear displacement curves

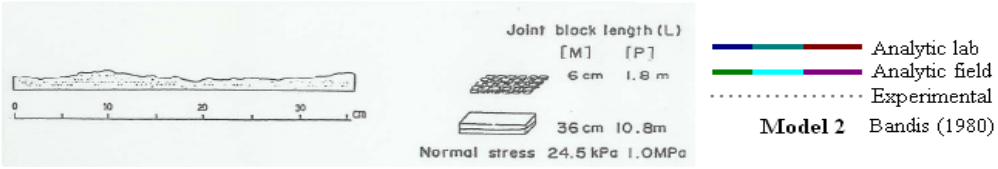

(e) Joint wall profile

(f) Input parameters used in simulation

Sample size cm	ϕ_r (o)	α_o (o)	λ cm	σ_c KPa	i_o —	λ_w —	η_i —
6	32	38	0.4	2000	—	—	—
36	32	38	0.4	2000	8	15	0.83 *

(g) Fitting constants

C cm	f_1 —	Ω —	R_f —	D —	κ —
0.4	0.219	12	0.9	0.45	16
0.4	0.219	12	0.9	0.45	16

* 2 contacts / (36/15) waves = 0.83

Figure 13. Comparison between proposed model and test results (experimental data from Bandis, 1980)

Fig. 14 shows the variation of the measured average angle of irregularities with the measuring interval for Model 1, as reported by Bandis (1980), along with the initial values (α_o, i_o) that match peak strength. This figure suggests that the initial asperity angle can be determined from the surface profile by extrapolating the curve of measured angles to a nil measuring interval.